Optics Letters

Efficient two-photon excitation by photonic dimers

YAO ZHOU,[1,†] ZIHAO CHEN,[1,†] LIHONG V. WANG,[2] AND JUNG-TSUNG SHEN[1,*]

[1]The Preston M. Green Department of Electrical and System Engineering, Washington University in St. Louis, St. Louis, Missouri 63130, USA
[2]Andrew and Peggy Cherng Department of Medical Engineering, California Institute of Technology, Pasadena, California 91125, USA
*Corresponding author: jushen@wustl.edu

Received 30 October 2018; revised 15 December 2018; accepted 15 December 2018; posted 17 December 2018 (Doc. ID 349506); published 16 January 2019

In this Letter, we show that photonic dimers, the quantum mechanical bound states of two photons, enable efficient nonlinear two-photon excitation, primarily due to the Lorentzian energy anti-correlation and to the temporal proximity between the constituent photons. We analytically and numerically demonstrate the order-of-magnitude improvement of the excitation efficiency per photon by the photonic dimers over the ultrashort pulses from a laser. We further show that, owing to the high excitation efficiency, the two-photon transition rate by photonic dimers deviates from the well-known linear intensity dependence at low intensities. Possible approaches for generating the photonic dimers in semiconductor platforms are also investigated.

https://doi.org/10.1364/OL.44.000475

Two-photon excitation (TPE) is a nonlinear process in which a fluorophore is excited by nearly simultaneous absorption of two lower-energy photons (typically in the infrared spectral range, in contrast to the UV energy photon in single-photon transition) via short-lived intermediate states. In two-photon fluorescence light microscopy [1], the use of a longer excitation wavelength leads to increased penetration because both the absorption and the reduced scattering coefficients are decreased, which makes three-dimensional *in vivo* imaging of thick cells and tissues at millimeter scales possible [2]. Nonetheless, because two-photon absorption has an exceedingly small two-photon cross section on the order of 1 GM (1 GM = 10^{-50} cm^4 s/photon) [3], ultrashort pulsed laser excitation is needed to deliver high-photon flux to the sample to generate efficient absorption. Even so, the excitation efficiency remains exceptionally low: for example, for a pulse containing 2.4×10^9 photons, merely 5.3×10^{-3} photons are absorbed per fluorophore under typical TPE conditions [4]. The finite quantum yield of the fluorophore (5% to 90%) further decreases the efficiency. To increase the TPE efficiency, it is required that the energies of the two incoming photons match the transition energy in the frequency domain and that the two photons arrive nearly simultaneously on the scale of the virtual state lifetime in the time domain. These two conditions obviously are incompatible for uncorrelated photons in an ultrashort pulse. TPE processes by entangled photon pairs have been investigated using the density matrix approach and second-order time-dependent perturbation [5–7]. However, the density matrix approach neglects the interferences between the atomic excitation amplitudes by different frequencies of the optical excitation field and, as shown below, the second-order perturbation is found to be too crude to be quantitatively correct. Moreover, in the seminal work of Ref. [5], a nearly resonant intermediate state is assumed, which in general is not valid in fluorophores used in the TPE microscopy. Here, we investigate the TPE processes by photonic bound states by explicitly including the interferences between the atomic excitations by all photonic frequencies. Our approach is applicable to a wide range of the intermediate state frequency detunings, including the far-off-resonance scenario that is directly relevant for TPE microscopy [1,2]. We show that the photonic bound states enable efficient nonlinear TPE per photon over the ultrashort pulses from a laser, primarily due to the Lorentzian energy anti-correlation and to the temporal proximity between the constituent photons. We further show that, owing to the high excitation efficiency, the two-photon transition rate by photonic bound states could deviate from the TPE linear intensity dependence [3,5].

The simplest realization of the photonic bound states is a photonic dimer consisting of two entangled photons [8–11]. The dimer is characterized by two time scales: the coherence time T (the temporal duration of each photon) and the correlation time τ (the temporal width of the relative wavefunction of the entangled photons). We now consider the TPE process by different optical excitation schemes. A fluorescence molecule in a single-mode optical waveguide [Fig. 1(a)] is excited by three different excitation optical fields incident from the left: a long 1 ns [Fig. 1(b)] and a short 200 fs [Fig. 1(c)] two-photon Gaussian pulse from a conventional laser, and a photonic dimer with a correlation time $\tau = 50$ ps and a coherence time $T =$ 1 ns [Fig. 1(d)]. The fluorophore is located at $x = 0$ and is modeled as a three-level system, where the ground state $|g\rangle$ (energy $\hbar\Omega_g$) and the excited state $|e\rangle$ (energy $\hbar\Omega_e$) have the same parity, so that single-photon transitions from $|g\rangle$ to $|e\rangle$ are parity forbidden, and only a two-photon excitation via an

intermediate state $|i\rangle$ (energy $\hbar\Omega_i$) is allowed. The intermediate state may represent one of complete sets of eigenstates, which have non-vanishing dipole matrix elements with $|g\rangle$ and $|e\rangle$. $\Omega_e - \Omega_g \equiv 2\Omega$ is the transition frequency. The frequency detuning of the intermediate state $|i\rangle$ is $\delta \equiv \Omega_i - \Omega_g - \Omega$.

The pulse consists of two identically overlapping Gaussian wavepackets with spatial width σ and central frequency Ω, and it is described by $\phi_{\text{in}}(x_1, x_2) = 1/(\sqrt{2\pi}\sigma)\exp[i\Omega(x_1 + x_2)/v_g - (x_1 - x_0)^2/4\sigma^2 - (x_2 - x_0)^2/4\sigma^2]$, where x_1 and x_2 correspond to the location of each photon in the input port of the waveguide, and x_0 is the center position of the input pulse (the results will not depend on the choice of x_0 as long as the initial pulse does not overlap with the molecule). Such an input is a product state, so the two photons are uncorrelated. The coherence time is the full width at half-maximum of the pulse $T \equiv 2\sigma/v_g$. The Gaussian modulated dimer is described by $\phi_{\text{in}}(x_1,x_2) = N\exp[-\gamma|x_1 - x_2|/v_g + i\Omega(x_1 + x_2)/v_g - (x_1 - x_0)^2/4\sigma^2 - (x_2 - x_0)^2/4\sigma^2]$, where N is the normalization factor. The center frequency of each photon is Ω. The coherence time is $T = 2\sigma/v_g = 1$ ns, and the correlation time for the probability density is defined by $\tau \equiv 1/(2\gamma) = 50$ ps. For each case, the probability density $|\phi_{\text{in}}|^2$ is plotted [12]. Figure 1(e) plots the joint frequency spectrum of the dimer described in Fig. 1(d), exhibiting frequency anti-correlation along the $\omega_1 + \omega_2 = 2\Omega$ axis: when one photon has a frequency ω_1, the frequency of the other photon ω_2 is constrained to the value $2\Omega - \omega_1$, within the order of $1/T$. The anti-correlation takes place within the temporal window T. The Hamiltonian of the system is [13]

$$\frac{H}{\hbar} = \int \mathrm{d}x \Bigg\{ -iv_g c_R^\dagger(x)\frac{\partial}{\partial x}c_R(x) + iv_g c_L^\dagger(x)\frac{\partial}{\partial x}c_L(x) + \delta(x)\Bigg[\sum_{j=L,R} c_j(x)(V_1 a_i^\dagger a_g + V_2 a_e^\dagger a_i) + \text{h.c.}\Bigg]\Bigg\} + \Omega_g a_g^\dagger a_g + \Omega_i a_i^\dagger a_i + (\Omega_e + \Delta_a - i\gamma_a)a_e^\dagger a_e, \quad (1)$$

where the first two terms describe the waveguided photons propagating in the right and left directions, respectively, with a group velocity v_g. $c_R^\dagger(x)(c_R(x))$ is the creation (annihilation) operator for the right-moving photon, and $c_L^\dagger(x)(c_L(x))$ is similarly defined for the left-moving photon. The next term

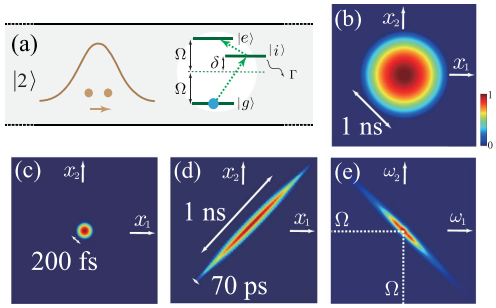

Fig. 1. Two-photon excitation process. (a) A two-photon pulse interacting with a fluorescent molecule. (b), (c), (d) Probability density plots of two-photon optical excitation in time scale. (b) A long Gaussian pulse with $T = 1$ ns. (c) A short Gaussian pulse with $T = 200$ fs. (d) A photonic dimer with $T = 1$ ns and $\tau = 50$ ps. (e) Joint-frequency spectrum of the photonic dimer described in (d). All density plots are normalized to the same color range.

describes the absorption of a photon and the excitation of the molecule from $|g\rangle$ to $|i\rangle$ with a coupling strength V_1, or from $|i\rangle$ to $|e\rangle$ with V_2. $a_{g,i,e}^\dagger(a_{g,i,e})$ is the creation (annihilation) operator of the corresponding state. The h.c. term refers to the Hermitian conjugate. The last three terms describe the energy of molecular states. The molecular energy renormalization $\Delta_a - i\gamma_a$ results from coupling with the ambient environment [13,14], which accounts for the dissipation and dephasing of the excited state. The renormalization term is omitted here. To simplify the description, we assume that $V_1 = V_2 = V$. The decay rate of the excited states into the waveguided mode is $\Gamma = V^2/v_g$, and the spontaneous emission lifetime of the molecule is $\tau_0 = 1/\Gamma$ [8,9], which is taken to be 100 ps.

The scattering process is given by the Schrödinger equation $i\hbar\partial_t|\phi(t)\rangle = H|\phi(t)\rangle$, where the wavefunction $|\phi(t)\rangle$ describes both the photons and the fluorescent molecule, with the specified photonic excitation and the molecular state as the initial conditions. The equations of motion are evolved numerically in time to trace out the full spatiotemporal dynamics of the scattering process [15]. In particular, the excitation amplitude $e_a(t)$ of the excited molecular state $|e\rangle$ is recorded for each excitation scheme (dimer, Δ; long pulse, ○; short pulse, +). Figure 2(a) plots the excitation efficiency $\int |e_a(t)|^2\mathrm{d}t$ (the integration is over the duration of the optical excitation). As the excitation efficiency is the number of photons absorbed per fluorophore, it can be shown to be related to the two-photon cross section σ_{2p} as $\int |e_a(t)|^2\mathrm{d}t = \sigma_{2p}/(TA^2)$, where A is the diffraction-limited area of the pulse [4]. Multiplied by the quantum yield η, the quantity $\eta\int |e_a(t)|^2\mathrm{d}t$ is proportional to the number of fluorescence photons (fluorescence signal strength). Numerically, it is found that, up to $\delta \simeq 4\Gamma$ (small-detuning limit), the excitation efficiency of the dimer outperforms that of the short and the long pulses. As the detuning is much less than the frequency bandwidth of the short pulse (1.6%), the excitation efficiency by a short pulse remains constant in Fig. 2(a). The excitation efficiency of the photonic dimer and the long pulse, however, decreases gradually. For large frequency detuning, as is the case for typical fluorescence molecules ($\delta \simeq 10^4\Gamma$), the excitation efficiency for all schemes becomes exponentially small, and an accurate numerical computation of the efficiency is extremely challenging. In the following, we present a time–frequency conjugate (TFC) model for computing the excitation efficiency. As will be seen below, at the small-detuning limit, the TFC model agrees well with the rigorous numerical results for all three excitation schemes, while at the large-detuning limit, the predicted short-pulse excitation efficiency is compatible with the results inferred from the experiments.

The TFC model incorporates the pulse nature to account for TPE in both the time and the frequency domain. In the time domain, the joint probability density of two photons to arrive at the fluorescence molecule is given by the second-order correlation function $G^{(2)}(t_1, t_2) \equiv \langle\phi_{\text{in}}|\hat{a}^\dagger(t_2)\hat{a}^\dagger(t_1)\hat{a}(t_1)\hat{a}(t_2)|\phi_{\text{in}}\rangle$, where $|\phi_{\text{in}}\rangle$ is the input two-photon state, and $\hat{a}(t_1)$ is the photon annihilation operator evaluated at the location of the fluorescence molecule. We consider the two-photon excitation process $|g\rangle \to |i\rangle \to |e\rangle$ as two successive single-photon transitions, each between a pair of energy levels ($|g\rangle$ to $|i\rangle$ then to $|e\rangle$), with the second transition being conditioned by the occurrence of the first transition

(Fig. 1). As the intermediate state couples to the waveguide and the environment, thus a spontaneous decay with a lifetime τ_0 takes place after being excited by the first photon at t_1, and the amplitude of the intermediate state $|i\rangle$ of the molecule becomes $e^{-(t_2-t_1)/\tau_0}$ when the second photon arrives at t_2. In the frequency domain, the excitation amplitude for a single-photon two-level transition is given by $A_{+\delta}(\omega) = \sqrt{\Gamma}/(\omega - \Omega - \delta + i\Gamma)$ [16], where ω is the frequency of the illuminating photon, and δ is the frequency detuning. Combining these considerations, the two-photon excitation efficiency is proportional to $P_t \times P_f$, where

$$P_t = \int_{-\infty}^{+\infty} \mathrm{d}t \int_0^{+\infty} \mathrm{d}\Delta t G^{(2)}(t, t+\Delta t) e^{-\Gamma \Delta t}, \tag{2}$$

$$P_f = \left| \int \frac{\mathrm{d}\omega_1 \mathrm{d}\omega_2}{2\pi} F(\omega_1) A_{+\delta}(\omega_1) F(\omega_2|\omega_1) A_{-\delta}(\omega_2) \right|^2, \tag{3}$$

where $\Delta t \equiv t_2 - t_1$, $F(\omega_1)$ is the frequency distribution of the first arrival photon, and $F(\omega_2|\omega_1)$ is the conditional frequency distribution of the second photon. We apply the TFC model to all three excitation schemes. For the Gaussian pulses, the two photons are independent, and one has $F(\omega_2|\omega_1) = F(\omega_2)$. Thus the excitation efficiency is

$$\kappa \left(\iint \frac{2}{\pi T^2} e^{-\frac{2(t-t_0)^2}{T^2} - \frac{2(t+\Delta t-t_0)^2}{T^2} - \frac{\Delta t}{\tau_0}} \mathrm{d}\Delta t \mathrm{d}t \right) \times \left| \iint \frac{\mathrm{d}\omega_1 \mathrm{d}\omega_2}{(2\pi)^2} \frac{e^{-(\omega_1-\Omega)^2\frac{T^2}{4} - (\omega_2-\Omega)^2\frac{T^2}{4}} T\Gamma}{(\omega_1 - \Omega - \delta + i\Gamma)(\omega_2 - \Omega + \delta + i\Gamma)} \right|^2, \tag{4}$$

where the proportionality κ accounts for all other matrix elements of the transitions (to be determined numerically), and $t_0 = -x_0/v_g$ is an irrelevant reference point. All variables can be rescaled by $\Gamma = 1/\tau_0$. In contrast, for a two-photon dimer, the frequency distribution is essentially determined by the Fourier transform of the relative wavefunction when $\tau \ll T$:

$$\int_{-\infty}^{+\infty} \int_{-\infty}^{x_1} \frac{\mathrm{d}x_1 \mathrm{d}x_2}{2\pi} N' e^{-\frac{\gamma}{v_g}(x_1-x_2) + i\frac{\Omega}{v_g}(x_1+x_2) - ik_1 x_1 - ik_2 x_2} = \frac{N'}{\gamma + i(\omega_1 - \Omega)} \delta(\omega_1 + \omega_2 - 2\Omega), \tag{5}$$

where N' is a normalization factor, and $\omega_{1,2} = k_{1,2} v_g$. The frequency distribution of the first photon is Lorentzian with $F(\omega_1) = N'/(\gamma + i(\omega_1 - \Omega))$ and of the second photon is $F(\omega_2|\omega_1) = \delta(\omega_1 + \omega_2 - 2\Omega)$. Thus the excitation efficiency becomes

$$\kappa \left(\iint |N'|^2 e^{-\frac{4(t-t_0)^2}{T^2} - \frac{4\Delta t(t-t_0)}{T^2} - \frac{\Delta t}{\tau_0} - \frac{\Delta t}{\tau}} \mathrm{d}\Delta t \mathrm{d}t \right) \times \left| \int \frac{d\omega}{2\pi} \frac{iN'\Gamma}{(\omega - \Omega - i\gamma)[(\omega - \Omega - \delta)^2 + \Gamma^2]} \right|^2. \tag{6}$$

The temporal part is approximately equal to $|N'|^2 T\sqrt{\pi}/(2/\tau_0 + 2/\tau)$ when $\tau \ll T$ (the limit of practical interest). For large detuning, $P_f \propto 1/\delta^2$ as the integrand is maximized at $\omega = \Omega + \delta$. In contrast, for short pulses, $P_f \propto 1/\delta^4$, which is much smaller than a dimer for large δ.

Here we compute the TPE efficiency by the spontaneous parametric down-converted photon pairs (SPDC), which are also frequency anti-correlated, but with a Gaussian distribution: $\phi_{\mathrm{in}}(x_1, x_2) = N'' \exp[-(x_1 - x_2)^2/4\sigma_s^2 + i\Omega(x_1 + x_2)/v_g - (x_1 - x_0)^2/4\sigma^2 - (x_2 - x_0)^2/4\sigma^2]$ with a coherence time $T = 2\sigma/v_g$, a correlation time $\tau = 2\sigma_s/v_g$, and a normalization factor N''. In the long pulse approximation ($T \gg \tau$), one has $F(\omega_2|\omega_1) = \delta(2\Omega - \omega_1 - \omega_2)$, and the excitation efficiency for SPDC photon pair is

$$\kappa \left(\iint |N''|^2 e^{-\frac{2(t-t_0)^2}{T^2} - \frac{2(t+\Delta t-t_0)^2}{T^2} - \frac{\Delta t}{\tau_0} - \frac{\Delta t^2}{\tau^2}} \mathrm{d}\Delta t \mathrm{d}t \right) \times \left| \int \frac{\mathrm{d}\omega}{2\pi} \frac{N''\sqrt{\pi}\tau\Gamma e^{-\tau^2(\omega-\Omega)^2/4}}{[(\omega - \Omega - \delta)^2 + \Gamma^2]} \right|^2. \tag{7}$$

The excitation efficiency of the SPDC photon pair is also plotted in Fig. 2 (SPDC:×), with the same correlation time 50 ps. For small detuning ($\delta \lesssim 5\Gamma$), a SPDC photon pair is as efficient as a dimer. However, for large detuning ($\delta \gtrsim 10^2\Gamma$), the SPDC frequency distribution decays exponentially, resulting in an exponentially small amplitude ($\propto e^{-\tau^2\delta^2/4}$) at the transition resonance ($\omega \approx \Omega \pm \delta$); it turns out that the amplitude at the photon center frequency ($\omega \approx \Omega$) dominates, which is $\propto 1/\delta^2$. Consequently, the SPDC photon pair is also frequency anti-correlated, $P_f \propto 1/\delta^4$. We note that if the interferences between the atomic excitation amplitudes are neglected, one obtains an overestimated efficiency $P_f \propto 1/\delta^2$ [6].

The TFC model described above provides the key tool for investigating the excitation efficiency at a large-detuning limit that is beyond the *ab initio* computational approach. Figure 2(b) plots the excitation efficiency over a wide range of δ up to $10^6\Gamma$ for all excitation schemes. The unknown constants κ, N', and N'' are fixed by equating to the rigorous numerical results at only one point at $\delta = 0$. The excitation efficiencies given by the numerical results and by the TFC

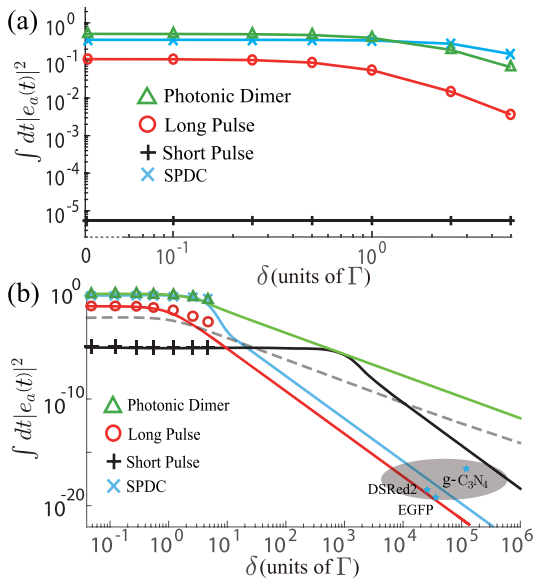

Fig. 2. Excitation efficiency. (a) Numerical results (marks on the curves) of the excitation efficiency for various excitation schemes at the small-detuning regime. (b) The time–frequency conjugate model (solid curves). The shaded area represents the range of the efficiency of three fluorophores (proteins EGFP and DSRed2, and quantum dot g-C_3N_4) estimated from experimental data. The dashed curve is the result of the semiclassical second-order perturbation.

model agree well throughout the small-detuning limit range. The efficiency for the 1-ns-long pulse decreases rapidly at approximately $\delta \simeq 10\Gamma$, while the efficiency for the 200 fs short pulse eventually degrades at approximately $\delta \simeq 10^3\Gamma$. In the figure, the efficiency of three representative fluorophores (proteins EGFP and DSRed2, and quantum dot g-C_3N_4) is estimated from available experiments [17,18] via the aforementioned relation between the two-photon cross-section σ_{2p} and the excitation efficiency. At $\delta \simeq 10^4\Gamma$, the dimers provide a three-orders-of-magnitude improvement in the excitation efficiency. We note that these fluorophores are off-resonance with a large intermediate frequency detuning $\delta\tau \simeq 5 \times 10^3$, which is beyond the applicability of the calculations in Ref. [5] that assumes the limit $\delta\tau \ll 1$. In Fig. 2(b), we also provide the results using the semi-classical single-frequency second-order perturbation method (dashed curve). We also found numerically that the excitation efficiency by the photonic dimers can be further increased when the correlation time τ decreases when δ is large. For a pulse containing N photon pairs, by assuming that each pair interacts with the molecule independently, the total excitation efficiency P_N is given by a simple probabilistic model as $P_N = 1 - (1 - P)^N$, where $P = \int |e_a(t)|^2 dt$ is the single pair excitation efficiency. For a typical pulse containing $N = 10^9 \sim 10^{13}$ photon pairs, since P is $\lesssim 10^{-13}$, a short pulse or SPDC light, $P_N \approx NP$, that is, the well-known TPE linear intensity dependence is recovered [3,5]. However, when P is enhanced to $\gtrsim 10^{-10}$ as is in the case for the dimer, $P_N \approx 1 - e^{-NP}$, which deviates from the linear intensity dependence.

The first experimental confirmation of the photonic dimers is in the cold atom system [10]. Here we investigate two approaches for generating dimers in solid-state platforms. The first approach is to launch a single resonant photon to interact with an excited quantum dot (QD) (spontaneous lifetime τ_0) in a waveguide [Fig. 3(a)]. Figure 3(b) plots the two-photon probability density after scattering for the case $T = 0.6\tau_0$. The first quadrant (RR branch) depicts two transmitted photons to the right of the QD. To quantify the generation efficiency, we define the forward efficiency

$$\xi_f \equiv \frac{\int dE |\langle B_E | \phi(t \to +\infty)\rangle_{RR}|^2}{{}_{RR}\langle \phi(t \to +\infty) | \phi(t \to +\infty)\rangle_{RR}},$$

where $|B_E\rangle$ is the unmodulated photonic dimer state of energy E [9] and $|\phi(t \to +\infty)\rangle_{RR}$ is the two-photon wavefunction in the forward RR branch. ξ_f gives the weight of the photonic dimer in the forward scattering two-photon wavepacket. Another useful matric is the total efficiency ξ_t, which is defined by using the full-space state $|\phi(t \to +\infty)\rangle$ (in all four quadrants) in the denominator instead. By varying the coherence time T of the input, the maximum value of ξ_f for the first approach [red curve in Fig. 3(c)] reaches 71% when $T = 0.6\tau_0$, and ξ_t (black curve) reaches 35% when $T = 0.36\tau_0$. In the second approach a two-photon Fock state is injected to interact with a ground state QD [Fig. 3(d)]. Figure 3(e) plots the probability density for the case $T = 10\tau_0$, and Fig. 3(f) plots the generation efficiencies. For the second approach, although ξ_t can reach nearly 100% for large T, ξ_t however is small as it is limited by the low two-photon transmission. As the correlation time of the generated photonic dimers is determined by the spontaneous emission time of the quantum emitter, photonic dimers with an ultrashort correlation time could be generated using ultra-fast (<11 ps) yet efficient sources of spontaneous emission [19], which further increases the excitation efficiency.

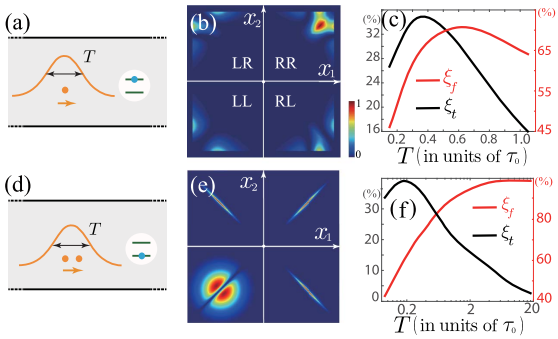

Fig. 3. Generation of photonic dimers. (a) Generation via stimulated emission: a resonant Gaussian photon $\phi_{in}(x) = (1/2\pi\sigma^2)^{1/4} e^{-(x-x_0)^2/4\sigma^2} e^{i\Omega x}$ is incident on an excited QD. (b) Two-photon probability density after scattering for $T = 0.6\tau_0$. (c) Total generation efficiency ξ_t (black curve, left axis) and forward generation efficiency ξ_f (red curve, right axis) of approach (a). (d) Generation via a two-photon Gaussian Fock state interacting with a ground-state QD. (e) Two-photon probability density after scattering for $T = 10\tau_0$. The transmitted (reflected) photons exhibit bunching (anti-bunching) statistics. (f) Generation efficiencies of approach (d).

Funding. National Science Foundation (NSF); Directorate for Engineering (ENG) and Division of Electrical, Communications and Cyber Systems (ECCS) (1608049, 1838996).

†These authors contributed equally to this Letter.

REFERENCES

1. W. Denk, J. Strickler, and W. Webb, Science **248**, 73 (1990).
2. D. Kobat, N. G. Horton, and C. Xu, J. Biomed. Opt. **16**, 106014 (2011).
3. C. Xu and W. W. Webb, J. Opt. Soc. Am. B **13**, 481 (1996).
4. L. Wang and H. Wu, *Biomedical Optics: Principles and Imaging* (Wiley, 2007).
5. J. Javanainen and P. L. Gould, Phys. Rev. A **41**, 5088 (1990).
6. H. You, S. M. Hendrickson, and J. D. Franson, Phys. Rev. A **80**, 043823 (2009).
7. R. de J León-Montiel, J. Svozilík, L. J. Salazar-Serrano, and J. P. Torres, New J. Phys. **15**, 053023 (2013).
8. J.-T. Shen and S. Fan, Phys. Rev. Lett. **98**, 153003 (2007).
9. J.-T. Shen and S. Fan, Phys. Rev. A **76**, 062709 (2007).
10. O. Firstenberg, T. Peyronel, Q.-Y. Liang, A. V. Gorshkov, M. D. Lukin, and V. Vuletic, Nature **502**, 71 (2013).
11. Y. Shen and J.-T. Shen, Phys. Rev. A **92**, 033803 (2015).
12. M. Bradford and J.-T. Shen, Opt. Lett. **39**, 5558 (2014).
13. J.-T. Shen and S. Fan, Phys. Rev. A **79**, 023837 (2009).
14. Z. Chen, Y. Zhou, and J.-T. Shen, Opt. Lett. **42**, 887 (2017).
15. M. Bradford and J.-T. Shen, Phys. Rev. A **85**, 043814 (2012).
16. J.-T. Shen and S. Fan, Phys. Rev. Lett. **95**, 213001 (2005).
17. M. Drobizhev, N. S. Makarov, S. E. Tillo, T. E. Hughes, and A. Rebane, Nat. Methods **8**, 393 (2011).
18. X. Zhang, H. Wang, H. Wang, Q. Zhang, J. Xie, Y. Tian, J. Wang, and Y. Xie, Adv. Mater. **26**, 4438 (2014).
19. T. B. Hoang, G. M. Akselrod, C. Argyropoulos, J. Huang, D. R. Smith, and M. H. Mikkelsen, Nat. Commun. **6**, 1 (2015).